Microtearing modes at the top of the pedestal

D Dickinson[1], C M Roach[1], S Saarelma[1], R Scannell[1], A Kirk[1] and H R Wilson[2]

[1] EURATOM/CCFE Association, Abingdon, Oxon, OX14 3DB, UK.
[2] York Plasma Institute, Department of Physics, University of York, York, YO10 5DD, UK

E-mail: david.dickinson@ccfe.ac.uk

PACS numbers: 52.25.Fi, 52.30.Gz, 52.35.Lv, 52.35.Qz, 52.55.Fa, 52.65.Tt

Abstract. Microtearing modes (MTMs) are unstable in the shallow gradient region just inside the top of the pedestal in the spherical tokamak experiment MAST, and may play an important role in the pedestal evolution. The linear properties of these instabilities are compared with MTMs deeper inside the core, and further detailed investigations expose the basic drive mechanism. MTMs near the MAST pedestal top are not well described by existing theories. In particular the growth rate of the dominant edge MTM does not peak at a finite collision frequency, as frequently reported for MTMs further into the core. Our study suggests that the edge MTM is driven by a collisionless trapped particle mechanism that is sensitive to magnetic drifts. This drive is enhanced in the outer region of MAST by a high magnetic shear and a high trapped particle fraction. Observations of similar modes on conventional aspect ratio devices suggests this drive mechanism may be somewhat ubiquitous towards the edge of current day and future hot tokamaks.

1. Introduction

Initial analytic studies suggested that tearing modes should be stable at high binormal perpendicular wavenumber, k_y, due to increased field line bending [1], leading to a focus on larger scale, "gross" tearing modes. A kinetic study of the tearing mode found that an energy dependent collision operator could lead to an additional drive from the electron temperature gradient [2]. This drive can overcome the stabilising influence at large k_y, allowing unstable microtearing modes (MTMs) to exist. The parameter $\bar{\nu} = \nu_{ei}/\omega$, is important for MTMs, where ν_{ei} is the electron-ion collision frequency and ω is the frequency associated with the mode. Analytic treatments in the collisional ($\bar{\nu} \gg 1$), semi-collisional ($\bar{\nu} > 1$ and $\bar{\nu} \ll k_\parallel^2 v_{th,e}^2/\omega^2$) and collisionless ($\bar{\nu} \ll 1$) regimes were performed in slab geometry [3]. Here the instability arises due to the time dependent parallel thermal force providing an asymmetry in the parallel force on electrons as a consequence of the energy dependence of the collision operator [4, 5]. In the absence of collisions this asymmetry disappears and the slab drive is therefore expected to vanish for sufficiently small $\bar{\nu}$. Likewise large $\bar{\nu}$ becomes stabilising as the collisions prevent the electrons from building a perturbed current. Kinetic calculations in large aspect ratio toroidal geometry revealed an additional drive mechanism that depends on trapped particles and is effective in the banana regime, $\bar{\nu} < r/R = \epsilon$ [6].

The trapped particles themselves do not carry the perturbed current but collisions generate the instability by allowing current to grow in the barely passing particles close to the trapped-passing boundary, in a process that remains effective even for $\bar{\nu} \ll 1$. This effect is found, for realistic tokamak parameters, to be lost at higher collision frequencies in the collisionless regime, $\bar{\nu} < 1 < \bar{\nu}/\epsilon$ [7]. Importantly combining the slab and trapped particle drive mechanisms leads to an MTM growth rate which peaks for $\bar{\nu} \sim \mathrm{O}(1)$. Observations of a strong inverse collisionality dependence of the thermal confinement time made on both MAST [8] and NSTX [9] may be consistent with simulations showing MTM driven transport increasing with ν_{ei} [10].

Fully electromagnetic gyrokinetic simulations are now able to study microtearing modes numerically in experimentally relevant scenarios. Linear gyrokinetic calculations have found unstable MTMs in a wide range of equilibria including at mid-radius in spherical tokamaks (STs) [11–16], in simple large aspect ratio shifted circle model equilibria [15] and towards the edge in ASDEX Upgrade [17]. MTMs exhibit tearing parity, where in ballooning space the perturbed parallel magnetic vector potential, $\mathrm{A}_\parallel$, is even in the ballooning angle θ. This is associated with reconnection at the rational surfaces generating small scale island structures.

When the amplitude of these islands is sufficient they will overlap to generate a stochastic field, which gives rise to significant electron heat transport [18]. Estimates of the electron thermal diffusivity in NSTX based on a model of stochastic field transport [19] are found to be within a factor 2 of the experimental levels over a region in which MTMs are the dominant instability [20]. The first successful nonlinear simulations of microtearing turbulence [21, 22] indicate that, in the absence of sheared flows, the associated electron heat flux can indeed be significant, and within the range of experimental observations. The effect of sheared equilibrium flows is not yet clear, with conflicting findings emerging from these two studies. The dependence of this microtearing turbulence on electron beta, $\beta_e = 2\mu_0 n_e T_e/B^2$, inverse temperature length scale, $1/L_{T_e} = T_e'/T_e$, and collision frequency, ν_{ei} [10, 23] is broadly consistent with previous linear studies [15–17]. Whilst these gyrokinetic simulations agree qualitatively with the two drive mechanisms discussed earlier, through the dependence of the MTM growth rate, γ_{MTM}, on $\bar{\nu}$, the existence of a critical T_e' and the observation that $\omega \sim \omega_{*e}$, there is evidence that magnetic drifts, which have not been adequately treated analytically, are also important [15]. In particular, the energy dependence of the collision operator is vital for both analytic drives but in numerical simulations this had little impact in the presence of magnetic drifts [15]. Indeed it was found that both magnetic drifts and perturbed electrostatic potential, ϕ, could be destabilising, and in the absence of both of these effects the MTM was found to be stable [15]. It is likely that there are multiple mechanisms occurring simultaneously to drive (or damp) MTMs, with the local parameters determining the relative contribution of each mechanism. This can lead to different scaling of γ_{MTM}, depending upon which mechanism is dominant. For example, Ref. [23] notes that ϕ is destabilising for low safety factor, $q \lesssim 3$, but stabilising for $q \gtrsim 3$, suggesting that the dominant driving mechanism may be undergoing a transition as q varies. Whilst two MTM drive mechanisms have been uncovered by analytic theory, it is clear that additional mechanisms, related to the magnetic drifts, are absent from the existing literature.

Recent linear gyrokinetic studies of the pedestal in MAST [24] and JET [25] utilising the fully electromagnetic initial value gyrokinetic code GS2 [26] have found unstable MTMs in the shallow gradient region at the top of the pedestal, where they may play an important role in the pedestal evolution [27, 28]. These edge MTMs

exhibit some significant differences to the more familiar core MTMs, and this paper provides an in-depth study of the edge modes. A clear difference can be seen in ϕ, which is much less extended in θ in the edge case than in the core, as shown in figure 1. In both cases $A_\parallel$ is strongly peaked about $\theta = 0$, decaying by $\theta = \pm\pi$. This is a more extreme example of the comparison of MTM eigenfunctions on surfaces at $r/a = 0.6$ and $r/a = 0.8$ reported in Ref. [16]. It should be noted that the magnetic shear, $\hat{s}$, is

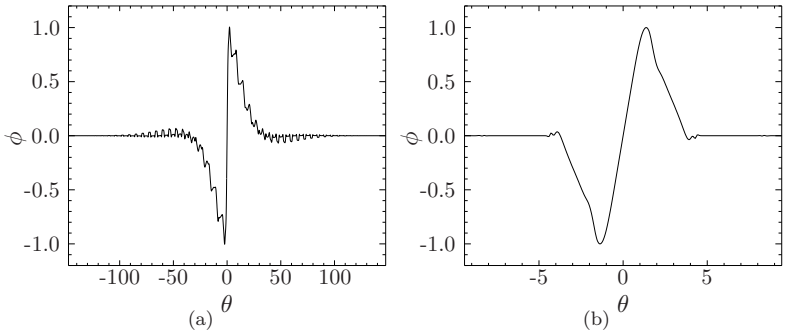

Figure 1. The electrostatic potential perturbation, ϕ, due to MTMs from linear GS2 simulations of MAST at (a) ψ_N=0.58 (shot #27905) and (b) ψ_N=0.94 (composite based on shots #24452, #24459 and #24763, see Ref. [24]).

much larger in the edge, and both eigenfunctions extend in the ballooning coordinate, θ, to approximately the same normalised radial wavenumber, $k_x\rho_i = \hat{s}\theta k_y \rho_i \sim 140$, where ρ_i is the ion Larmor radius. This is consistent with the mode extending until $k_x\delta_0 \sim \mathrm{O}(1)$, where δ_0 is the semi-collisional width [3]:

$$\delta_0 = L_s \frac{\sqrt{\omega_{*e}\nu_{ei}}}{k_y v_{th,e}} \tag{1}$$

with the shear length, $L_s = Rq/\hat{s}$. These cases are both in a similar collisionality regime as $\bar{\nu} = 0.26$ and 0.44 for the core and edge cases respectively.

In section 2 we introduce a local equilibrium from the MAST edge that is unstable to MTMs, and reduce this to a simpler model equilibrium with similar microstability properties. This provides a reference equilibrium for detailed linear gyrokinetic studies, presented in section 3, that probe the basic driving mechanisms for MTMs at the edge of MAST. Final conclusions are presented in section 4

2. Equilibrium parameters and simplifications

We base our studies on a reference local equilibrium from the plateau region at the top of a MAST H-mode pedestal, which is unstable to MTMs ‡. The reference flux surface is $\psi_N = 0.94$ at the midpoint during the ELM cycle, with the equilibrium parameters given in table 1. The growth rate spectrum is shown in figure 2(a). The minimal equilibrium conditions necessary to drive MTMs unstable are sought by progressively simplifying the equilibrium assumptions.

Sensitivity to flux surface shaping is investigated by fitting the reference MAST equilibrium using the s-α shifted concentric circle model [29]. This model allows easy independent control of the geometrical parameters affecting trapping, $\epsilon = r/R$, and

‡ A full account of the equilibrium reconstruction from MAST data is given in Ref. [24].

Table 1. Equilibrium parameters characteristic of MAST shot 24763 at the mid-point in time between two ELMs for $\psi_N = 0.94$.

q	$\hat{s}$	r/R	L_{ref}/L_T	L_r/L_n	β_e	α	$\nu_{ei}\left(v_{th,i}/L_{ref}\right)$
4.66	7.67	0.805	5.88	0.36	0.015	-5.66	1.98

the magnetic drifts, R, which shall later be shown to be crucial to the MTM instability studied here. The circle is a crude fit to the edge of MAST, as illustrated in figure 2(c) which compares this fit with the experimental flux surface. The γ_{MTM} spectrum for the circular fit is shown in figure 2(b). There is a significant shift in the $k_y\rho_i$ at which γ_{MTM} peaks relative to the shaped surface case, but the magnitudes of γ_{MTM} (and ω) are within a factor 2. This is consistent with previous studies showing that shaping is not essential for MTMs [15].

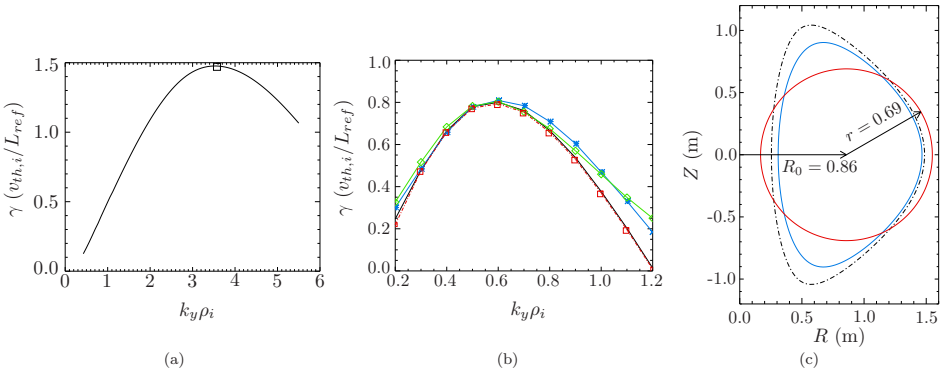

Figure 2. (a) γ_{MTM} spectrum for the MAST flux surface at $\psi_N = 0.94$, highlighting the peak wavenumber (□) corresponding to the ϕ eigenfunction of figure 1(b). (b) γ_{MTM} spectra for the circular equilibrium fit [—— in (c)] with: the standard full physics model excluding $B_\parallel$ (——); adiabatic ions (∗); including $B_\parallel$ (□) and neglecting ϕ (◇). (c) Circular fit (——) to the $\psi_N = 0.94$ flux surface (——) along with the last closed flux surface (— · —).

Figure 2(b) shows that calculations with fully kinetic and purely Boltzmann ion responses yield very similar γ_{MTM} spectra. Previous simulations of MTMs in the core also found that γ_{MTM} is insensitive to including fully kinetic ions as the ion response is close to Boltzmann [15–17]. In early kinetic treatment of the collisionless and semi-collisional MTMs the ion response was neglected [3], but can be strongly stabilising when $\rho_i > d$ [30], where d is the width of the current layer associated with the mode (e.g. the semi-collisional width, δ_0). Calculating the semi-collisional width for our reference equilibrium from (1) gives $\delta_0/\rho_i \sim \text{O}\left(10^{-3}\right)$ and with this current layer width the stabilising impact of the ion response is expected to be important [30].

The growth rate is insensitive to including compressional magnetic perturbations, $B_\parallel$, and only weakly sensitive to including the electrostatic potential, ϕ, which is slightly stabilising and has a modest impact on the frequency spectrum (not shown). Subsequent simulations in this paper will use the s-α equilibrium model, neglect the nonadiabatic ion response and $B_\parallel$, and retain ϕ due to its impact on ω at large $k_y\rho_i$.

The studies of section 3 are based on scans around the reference equilibium, during

which MTMs can become subdominant to other instabilities. GS2 is an initial value code, and subdominant MTMs are tracked, with this up-down symmetric equilibrium, by filtering to keep only the component of the nonadiabatic perturbed distribution function with odd parity in the parallel direction. These are tearing parity modes (i.e. modes where ϕ is odd and $A_\parallel$ is even about $\theta = 0$). Finally both the semi-collisional width, δ_0, and the collisionless width, $\delta_n = \rho_e\sqrt{2/\beta_e}$, are resolved by using a domain that is sufficiently extended in θ, $(-11\pi < \theta < 11\pi)$.

3. Linear mode analysis

There have been several linear gyrokinetic studies of how MTM stability depends on equilibrium parameters [15–17]. Here we explore a new region of parameter space, by moving to extremely low aspect ratio and high magnetic shear, which are typical of the MAST edge.

3.1. Temperature and density dependence

A finite electron temperature gradient is essential for both MTM drive mechanisms described in section 1, with the onset of instability arising above a certain threshold. The MTM real frequency, ω, is predicted to vary approximately linearly with the electron diamagnetic frequency, ω_{*e}, with a precise relationship that depends on the driving mechanism.

Scans have been performed by varying the normalised gradient length scales, L_{ref}/L_{T_e} and L_{ref}/L_{n_e} (with L_{ref} some reference length scale and $L_{n_e} = n_e'/n_e$), independently, at fixed values of all other parameters §. The resulting growth rate spectrum in figure 3(a) show a finite threshold temperature gradient that increases with k_y, and that $\gamma_{\rm MTM}$ increases monotonically above this threshold. Figure 3(b) shows that MTMs are unstable at $L_{ref}/L_{n_e} = 0$, and that $\gamma_{\rm MTM}$ is maximised at finite L_{ref}/L_{n_e} similar to previous findings [15, 16]. In both scans ω is found to be reasonably well described by $\omega_{*e}\,(a + b\eta_e)$ where $\eta_e = L_{n_e}/L_{T_e}$, in qualitative agreement with analytic predictions.

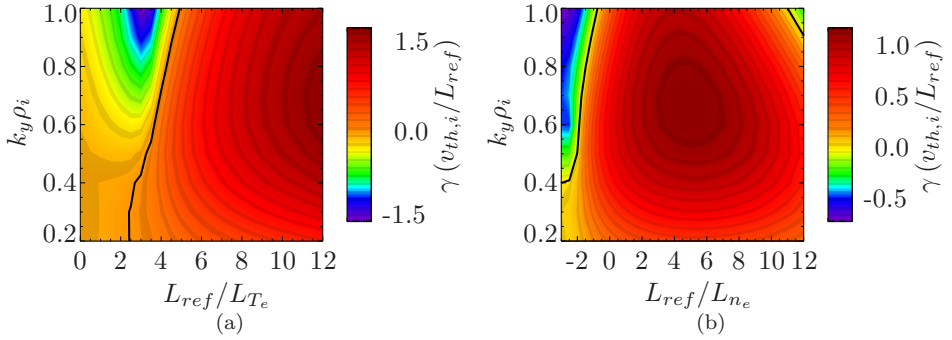

Figure 3. The growth rate as a function of $k_y\rho_i$ for varying (a) temperature and (b) density gradient length scales. The location of marginality, $\gamma_{\rm MTM} = 0$, is given (——).

§ The normalised pressure gradient, $\alpha = Rq^2\beta/L_p$, was held constant in these scans.

3.2. Beta

γ_{MTM} is insensitive to ϕ, and MTMs are driven by the magnetic perturbation, $A_{\parallel}$. Therefore γ_{MTM} will be strongly affected by β, which controls the strength of magnetic perturbations through Ampères law. Electromagnetic instabilities, like kinetic ballooning modes and MTMs, are typically unstable above a threshold β, with growth rates that then increase strongly with β [31]. This may explain discrepancies between different tokamaks in the observed confinement scaling with β [32]: increases in β that cross the threshold will increase transport whilst increases that remain below the threshold will have less impact (and may stabilise other instabilities [33, 34]).

The growth rates are shown for a range of k_y values in figure 4(a) for varying β_e (scaling α consistently). The variation seen here is somewhat complex, though some general remarks can be made. There is a clear stability threshold in β_e, which increases approximately linearly with k_y, above which γ_{MTM} increases rapidly with β_e. For sufficiently high β_e, further increases in β_e become stabilising, as was also seen in Ref. [15]. Varying α consistently with β_e significantly enhances the stabilisation at higher β_e, which is consistent with magnetic drifts becoming more favourable at higher α [35]. Holding α fixed in this scan, γ_{MTM} decreases more slowly with increasing β_e above the most unstable value, and furthermore the instability threshold moves to lower β_e. The local minimum in γ_{MTM} at $\beta_e \sim 0.022$ is only seen in the scan with α varying consistently, and not at fixed α.

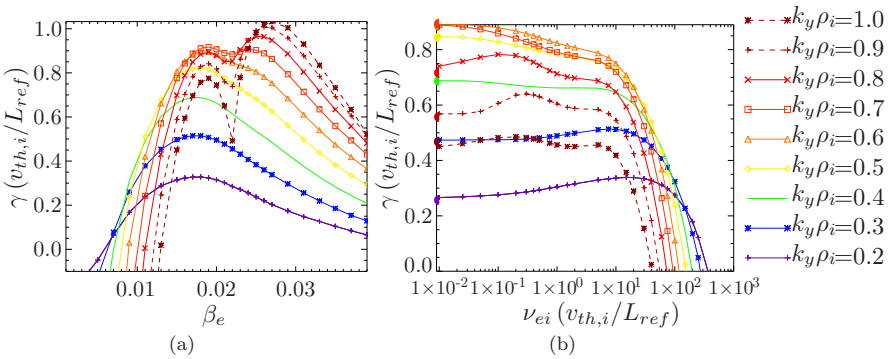

Figure 4. γ_{MTM} as a function of $k_y\rho_i$ and (a) β_e and (b) ν_{ei}. During the β_e scan the normalised pressure gradient, α, is varied consistently. The results of simulations with $\nu_{ei} = 0$ are shown in (b) by the filled semi-circles on the y-axis, indicating a substantial growth rate even in the absence of collisions. The key to the $k_y\rho_i$ values also applies to figures 5, 6, 7.

3.3. Collision frequency

It has already been pointed out that collisions play an essential role in the existing analytic drive mechanisms for MTMs. Linear gyrokinetic simulations have generally reported growth rates that peak for $\bar{\nu} \sim \text{O}\,(1)$, as may be expected from a mode driven by a combination of slab and trapped particle drives. Recent simulations have shown γ_{MTM} dropping by only a factor of 2, as ν_{ei} falls by over two orders of magnitude from its value at the peak [23], which suggests that as the collision based drive is removed, a further substantial drive mechanism remains.

Figure 4(b) shows γ_{MTM} as a function of ν_{ei} for each k_y. Increasing the collision frequency well above $\bar{\nu} \sim \text{O}(1)$ is stabilising. It is more striking that γ_{MTM} for the dominant mode, and at several other values of k_y, does not peak at finite ν_{ei}, but remains constant or even slowly increases as ν_{ei} decreases all the way to zero, which is in stark contrast to the "usual" behaviour ‖. The trapped particle drive mechanism of Ref. [6] must vanish at $\nu_{ei} \equiv 0$ as it requires collisions, and cannot therefore be responsible for the instability seen here. A **collisionless** mechanism is required, which cannot rely on the time-dependent thermal force.

Ref. [15] reported γ_{MTM} peaking at $\bar{\nu} \sim \text{O}(1)$ for mid-radius local equilibria in MAST, but closer to the MAST edge we find that γ_{MTM} peaks at $\nu_{ei} \sim 0$. Could this be explained by significant differences between the values of inverse aspect ratio, $\epsilon = r/R$, and magnetic shear, $\hat{s}$, at these two locations?

3.4. Aspect ratio (trapped particles)

Varying only the inverse aspect ratio, $\epsilon = r/R$, in the s-α model, corresponds to changing the trapped particle fraction whilst holding all other parameters fixed. This effectively scans in minor radius, r, at fixed R. The results from this scan, illustrated in figure 5(a), reveal a strong dependence of γ_{MTM} on ϵ, and suggest that trapped particles are important to the linear drive for the reference value of ν_{ei}. The decline in γ_{MTM} with decreasing ϵ is nearly uniform for $k_y \geq 0.5$, but rather weaker at lower k_y. This suggests that at low k_y the trapped particle drive may be complemented by another mechanism at the nominal ν_{ei}, which would also be consistent with figure 4(b).

Ref. [15] found that trapped particles are destabilising for $\bar{\nu} \ll 1$, but stabilising for $\bar{\nu} \gtrsim 0.5$ which is the reference collisionality regime here. Furthermore, the trapped particle drive was shown to be most effective at low ϵ (unlike in figure 5(a)). This is consistent with the trapped-passing boundary providing an instability drive, whilst the trapped particles are themselves stabilising owing to their inability to carry the current perturbation. The situation is different for MTMs at the MAST edge. Figure 5(a) suggests that trapped particles provide a direct MTM drive, and figure 4(b) shows that this survives without collisions.

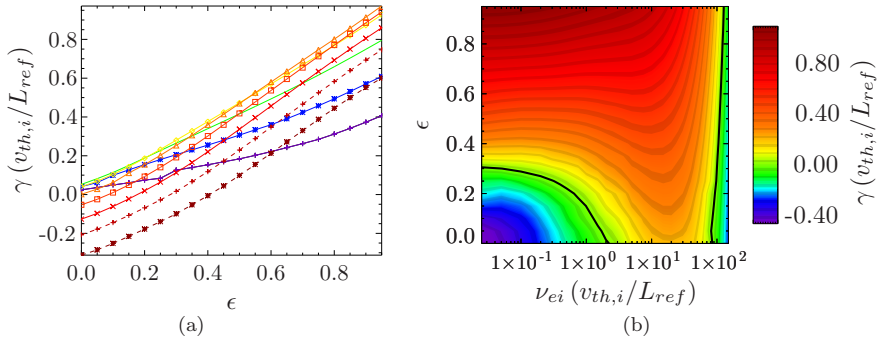

Figure 5. γ_{MTM} as the inverse aspect ratio, $\epsilon = r/R$, is varied for (a) $\nu_{ei} = 1.98$ at each k_y (k_y key given in figure 4) and (b) $k_y\rho_i = 0.6$ over a range of ν_{ei}, with —— indicating marginal stability. The frequency, ω, remains between -1.5 and -2.8 throughout these scans.

‖ γ_{MTM} for the lowest k_y mode peaks at finite ν_{ei}, and drops only slowly with decreasing ν_{ei}, closely resembling the dependence presented in Ref. [23].

Figure 5(b) shows how γ_{MTM} for the dominant mode, at $k_y\rho_i = 0.6$, depends on ν_{ei} and ϵ. The γ_{MTM} dependence on ϵ is strongest at low ν_{ei}. At low ϵ the growth rate maximises at $\nu_{ei} \sim \text{O}(10)$, but at high ϵ the growth rate peaks at the minimum ν_{ei}. Indeed for $\epsilon < 0.3$ the MTMs become stable for sufficiently small ν_{ei}, and a strong peak in γ_{MTM} is seen for $\bar{\nu} \sim 10$, which is consistent with previous findings [15, 16, 23]. The role of ϵ in enhancing γ_{MTM} should be most important near the pedestal region where the trapped particle fraction variation is maximised, especially in STs where ϵ approaches 1.

3.5. Safety factor and magnetic shear

The safety factor, q, and magnetic shear, $\hat{s}$, are significantly larger in the edge plateau of MAST than at the mid-radius surface studied in Ref. [15]. Figure 6(a) illustrates, for a range of k_y values, the complicated dependence of γ_{MTM} on q. γ_{MTM} exhibits multiple peaks at different q values, and these positions vary with k_y: e.g. the $k_y\rho_i$=1 mode has growth rate peaks at $q \sim 3$ and $q \sim 9$, and a local minimum at $q \sim 6$. Interestingly the MTM is stable for $q \lesssim 2$. These features may be related to the impact of q on bounce and transit frequencies, which are inversely proportional to q. Figure 6(b) shows results from a scan in $\hat{s}$, and clearly indicates a preferred value of $\hat{s}$ for which γ_{MTM} is maximised for each mode. The most unstable $\hat{s}$ decreases as k_y increases, and at lower $\hat{s}$ the peak of the γ_{MTM} spectrum moves to higher $k_y\rho_i$. Changes in $\hat{s}$ affect the magnetic drift frequency, ω_D, which in the next section will be shown to impact on the growth rate.

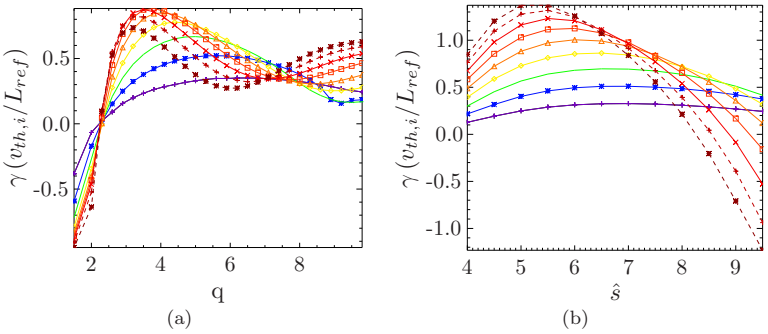

Figure 6. γ_{MTM} as a function of (a) q and (b) $\hat{s}$. The k_y key is given in figure 4

3.6. Drift frequency

In the s-α model the curvature and $\underline{\nabla}B$ drifts are equal, and for zero ballooning angle, $\theta_0 = 0$, are proportional to

$$D(\theta) = \epsilon_l \left[\cos(\theta) - (\alpha \sin(\theta) - \hat{s}\theta)\sin(\theta)\right] \tag{2}$$

where $\epsilon_l = 2L_{ref}/R$ determines the strength of the drifts. A scan in drift frequency was performed by varying ϵ_l around its reference value $\epsilon_l = 1.435$ with all other parameters fixed. Figure 7(a) shows that the growth rate peaks at a particular ϵ_l, which varies with k_y, and that γ_{MTM} is more sensitive to the drifts at higher k_y. The peak growth rate occurs at a drift strength factor that decreases approximately linearly with k_y, suggesting an optimal value of ω_D for which γ_{MTM} of each mode is

maximised. This indicates that some form of drift resonance may be important. In the absence of magnetic drifts (i.e. $\epsilon_l = 0$) the MTMs are stable, showing that the slab drive is insufficient for instability ¶.

Independent scans in the magnetic drift frequencies for trapped and passing particles, reveal that γ_{MTM} is only sensitive to the trapped particle drifts and that passing particle drifts are unimportant. We note that the previous scan in $\hat{s}$ was effectively a scan in the radial component of ω_D, as this is $\propto \sin(\theta)\,\hat{s}\theta$ (from (2)). Therefore the similarity of figures 6(b) and 7(a) indicate that the radial component of the magnetic drift is the dominant influence on the drive mechanism. In ballooning space the radial wavenumber exceeds k_y for $\hat{s}\theta > 1$, which arises for $\theta > 0.13$ in the edge, and for $\theta > 3.49$ for the mid-radius MAST parameters of Ref. [15]. The radial component of the drift frequency for trapped particles is clearly more significant at the edge of MAST than at mid-radius. Trapped particles and their radial drifts seem to play an essential role in the MTM drive mechanism at large ϵ. Analytic theories of the MTM either neglect the magnetic drift frequency, ω_D, or assume $\omega_D \ll \omega$. For MTMs at the edge of MAST it is demonstrated here that the magnetic drifts cannot be neglected.

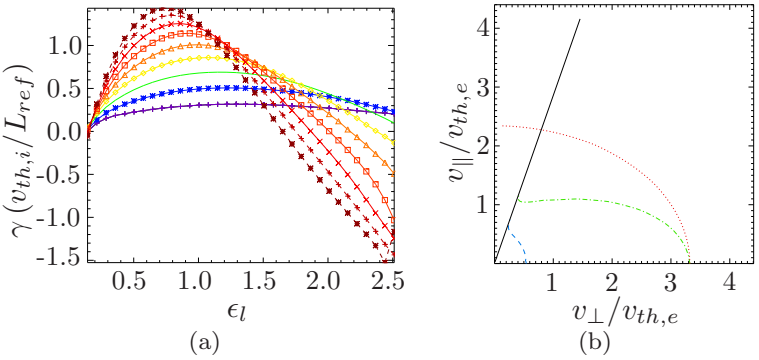

Figure 7. (a) γ_{MTM} as the normalised major radius, $\epsilon_l = 2L_{ref}/R$, is varied for fixed ϵ (k_y key given in figure 4) and (b) the location in velocity space where ω for $k_y\rho_i = 0.6$ matches the drift (evaluated at $\theta = 0$, ·····), precession (— · —) and bounce (- - - -) frequencies.

3.7. Frequencies

It is of direct interest to analytic theory to ask how the MTM mode frequency, ω, compares with the natural trapped particle frequencies: the bounce frequency, ω_b, drift frequency at $\theta = 0$, ω_D, and precession frequency, $\omega_p = \langle\omega_D\rangle$. The trapped particle frequencies depend on $v_\parallel$, $v_\perp$ and k_y. Figure 7(b) shows where in velocity space the trapped particle frequencies match the mode frequency for the $k_y\rho_i$=0.6 mode. The contours indicate that ω_D, ω_b and $\omega_p \sim \mathrm{O}(\omega)$ for a thermal particle, and that all three resonances lie within the range $0.5v_{th,e} - 3.5v_{th,e}$, and may therefore have significant impact.

This poses several thoughts for analytic theory. Firstly the perturbation changes significantly in one bounce period, due to the proximity of ω and ω_b. Bounce

¶ In Ref. [15] a residual instability remained in the absence of magnetic drifts (provided ϕ was retained), which may be due to a weaker stabilising effect from trapped particles at lower ϵ.

averaging, which is often used to simplify the trapped particle response, is therefore not appropriate here. Secondly the magnetic drift frequencies are of the same order as the mode frequency, and cannot be treated as small. Finally, with all three frequencies of the same order as the mode frequency, two or three wave resonances may be important.

4. Conclusions

Gyrokinetic simulations have found that microtearing modes (MTMs) are unstable in both STs and large aspect ratio devices. Recent simulations find that MTMs are also unstable in the shallow gradient region just inboard of the MAST H-mode pedestal, which may impact on its evolution between ELMs. Analytic theory has proposed two different linear drive mechanisms for MTMs: one based on a simple slab model, and the other requiring trapped particles. Both mechanisms require a finite rate of electron-ion collisions ($\nu_{ei} > 0$) for instability.

A detailed study of the basic linear properties of edge MTMs in MAST has been performed using a simplified circular s-α model equilibrium. Consistent with existing theories it is found that the mode frequency $\omega \sim \omega_{*e}$, and the modes are unstable only if finite stability thresholds are exceeded in dT_e/dr and β_e. The growth rate dependence on ν_{ei}, however, is in conflict with existing models. γ_{MTM} for the dominant mode is maximised in the absence of collisions (i.e. at $\nu_{ei} = 0$), where the existing drive mechanisms should vanish. Trapped particles are essential to drive these MTMs, and sensitivity of γ_{MTM} to the magnetic drift frequency suggests that a drift resonance may be involved. γ_{MTM} rises with the trapped particle fraction, and the $k_y\rho_i$ associated with the dominant mode drops with increasing $\hat{s}$. The mode frequency and the thermal trapped electron bounce, precession and drift frequencies are all of the same order. To our knowledge this regime has not been addressed by an existing analytic theory. In present models the magnetic drifts are typically neglected or treated as small, and any trapped particle response is usually obtained using bounce averaging. Neither of these approximations are valid here.

The drive for similar MTMs, at $k_y\rho_i \sim \mathrm{O}(1)$, should be enhanced in the high magnetic shear region of the edge plateau in tokamaks, and perhaps especially in STs. Similar MTMs have also recently been found unstable towards the edge of conventional aspect ratio tokamaks including JET [25, 36] and ASDEX Upgrade [17], suggesting that this neglected drive mechanism may have wide ranging significance.

Acknowledgments

The authors wish to thank J W Connor and R J Hastie for helpful discussions. This work was carried out using the HELIOS supercomputer system at International Fusion Energy Research Centre, Aomori, Japan, under the Broader Approach collaboration between Euratom and Japan, implemented by Fusion for Energy and JAEA. In addition the simulations presented here were enabled with access to the HECToR supercomputer through EPSRC Grant No. EP/H002081/1 and access to the high performance computing resources HPC-FF (Forschungszentrum Juelich). This work was partly funded by the RCUK Energy Programme under grant EP/I501045 and the European Communities under the contract of Association between EURATOM and CCFE. The views and opinions expressed herein do not necessarily reflect those of the European Commission.

References

[1] Furth H P, Killeen J and Rosenbluth M N 1963 *Phys. Fluids*, **6** 459–84

[2] Hazeltine R D, Dobrott D and Wang T S 1975 *Phys. Fluids* **18** 1778–1786

[3] Drake J F and Lee Y C 1977 *Phys. Fluids* **20** 1341–1353

[4] Hassam A B 1980 *Phys. Fluids* **23** 38–43

[5] Hassam A B 1980 *Phys. Fluids* **23** 2493–2497

[6] Catto P J and Rosenbluth M N 1981 *Phys. Fluids* **24** 243–255

[7] Connor J W, Cowley S C and Hastie R J 1990 *Plasma Phys. Control. Fusion* **32** 799–817

[8] Valovič M *et al* 2011 *Nucl. Fusion* **51** 073045

[9] Kaye S M *et al Nucl. Fusion* **47** 499–509

[10] Guttenfelder W *et al Phys. Plasmas* **19** 056119

[11] Kotschenreuther M, Dorland W, Liu Q P, Zarnstorff M C, Miller R L and Lin-Liu Y R 2000 *Nucl. Fusion* **40** 677–684

[12] Applegate D J *et al* 2004 *Phys. Plasmas* **11** 5085

[13] Wilson H R *et al* 2004 *Nucl. Fusion* **44** 917–929

[14] Roach C M *et al* 2005 *Plasma Phys. Control. Fusion* **47** B323–B336

[15] Applegate D J *et al* 2007 *Plasma Phys. Control. Fusion* **49** 1113–1128

[16] Guttenfelder W, Candy J, Kaye S M, Nevins W M, Bell R E and Hammett G W 2012 *Phys. Plasmas* **19** 022506

[17] Told D, Jenko F, Xanthopoulos P, Horton L D and Wolfrum E 2008 *Phys. Plasmas* **15** 102306

[18] Stix T 1973 *Phys. Rev. Lett.* **30** 833–835

[19] Rechester A and Rosenbluth M N 1978 *Phys. Rev. Lett.* **40** 38–41

[20] Wong K, Kaye S M, Mikkelsen D, Krommes J, Hill K, Bell R E and LeBlanc B 2007 *Phys. Rev. Lett.* **99** 135003

[21] Doerk H, Jenko F, Pueschel M J and Hatch D 2011 *Phys. Rev. Lett.* **106** 155003

[22] Guttenfelder W *et al Phys. Rev. Lett.* **106** 155004

[23] Doerk H, Jenko F, Gorler T, Told D, Pueschel M J and Hatch D R 2012 *Phys. Plasmas* **19** 055907

[24] Dickinson D, Saarelma S, Scannell R, Kirk A, Roach C M and Wilson H R 2011 *Plasma Phys. Control. Fusion* **53** 115010

[25] Saarelma S, Beurskens M N A, Dickinson D, Kirk A, Leyland M, and Roach C M 2012 In *Proc. 39th EPS Conf. on Plasma Physics*

[26] Kotschenreuther M, Rewoldt G and Tang W M 1995 *Comput. Phys. Commun.* **88** 128–140

[27] Dickinson D, Roach C M, Saarelma S, Scannell R, Kirk A and Wilson H R 2012 *Phys. Rev. Lett.* **108** 135002

[28] Roach C M, *In preparation*

[29] Connor J W, Hastie R J and Taylor J B 1978 *Phys. Rev. Lett.* **40** 396–399

[30] Cowley S C, Kulsrud R M and Hahm T S 1986 *Phys. Fluids* **29** 3230

[31] Snyder P B and Hammett G W 2001 *Phys. Plasmas* **8** 744

[32] Petty C C 2008 *Phys. Plasmas* **15** 080501

[33] Tang W M, Rewoldt G, Cheng C Z and Chance M S 1985 *Nucl. Fusion* **25** 151–164

[34] Belli E A and Candy J 2010 *Phys. Plasmas* **17** 112314

[35] Roach C M, Connor J W and Janjua S 1995 *Plasma Phys. Control. Fusion* **37** 679–698

[36] Saarelma S, *In preparation*